Atmospheric Tides in the Latest Generation of Climate Models

Citation: Covey, Curt, Aiguo Dai, Richard S. Lindzen, and Daniel R. Marsh. "Atmospheric Tides in the Latest Generation of Climate Models." J. Atmos. Sci. 71, no. 6 (June 2014): 1905–1913. © 2014 American Meteorological Society

As Published: http://dx.doi.org/10.1175/jas-d-13-0358.1

Publisher: American Meteorological Society

Persistent URL: http://hdl.handle.net/1721.1/92661

Version: Final published version: final published article, as it appeared in a journal, conference proceedings, or other formally published context

Atmospheric Tides in the Latest Generation of Climate Models*

CURT COVEY

Program for Climate Model Diagnosis and Intercomparison, Lawrence Livermore National Laboratory, Livermore, California

AIGUO DAI

University at Albany, State University of New York, Albany, New York

RICHARD S. LINDZEN

Massachusetts Institute of Technology, Cambridge, Massachusetts

DANIEL R. MARSH

National Center for Atmospheric Research,+ Boulder, Colorado

(Manuscript received 8 November 2013, in final form 26 February 2014)

ABSTRACT

For atmospheric tides driven by solar heating, the database of climate model output used in the most recent assessment report of the Intergovernmental Panel on Climate Change (IPCC) confirms and extends the authors' earlier results based on the previous generation of models. Both the present study and the earlier one examine the surface pressure signature of the tides, but the new database removes a shortcoming of the earlier study in which model simulations were not strictly comparable to observations. The present study confirms an approximate consistency among observations and all model simulations, despite variation of model tops from 31 to 144 km. On its face, this result is surprising because the dominant (semidiurnal) component of the tides is forced mostly by ozone heating around 30–70-km altitude. Classical linear tide calculations and occasional numerical experimentation have long suggested that models with low tops achieve some consistency with observations by means of compensating errors, with wave reflection from the model top making up for reduced ozone forcing. Future work with the new database may confirm this hypothesis by additional classical calculations and analyses of the ozone heating profiles and wave reflection in Coupled Model Intercomparison Project (CMIP) models. The new generation of models also extends CMIP's purview to free-atmosphere fields including the middle atmosphere and above.

1. Introduction

This paper updates our earlier study of atmospheric tides in climate-oriented general circulation models (Covey et al. 2011, hereafter CDML). The tides interact with surface and higher-altitude processes that play important roles in atmospheric dynamics and climate. CDML found a surprising consistency of model simulations with each other and with observations. The tides are driven in large part by solar heating of the ozone layer, which occurs in the altitude range 30–70 km (Chapman and Lindzen 1970), yet many of the models have a limited vertical domain that does not include the full range. CDML's results were consistent with previous work dating back to Lindzen et al. (1968) suggesting that when a model's upper boundary is placed at low altitude, a cancellation of errors can occur—reducing the forcing of tides by ozone heating, but also introducing spurious waves by reflection at the top boundary.

A significant shortcoming of CDML arose from a limitation of its model output database [Intergovernmental

Denotes Open Access content.

* Supplemental information related to this paper is available at the Journals Online website: http://dx.doi.org/10.1175/JAS-D-13-0358.s1.

+ The National Center for Atmospheric Research is sponsored by the National Science Foundation.

Corresponding author address: Curt Covey, LLNL Mail Code L-103, 7000 East Avenue, Livermore, CA 94550.
E-mail: covey1@llnl.gov

DOI: 10.1175/JAS-D-13-0358.1

TABLE 1. CMIP5 models for atmospheric tide studies.

	Model	Top full, half level	Layers*
1	BCC-CSM1.1	3.6, 2.2 hPa (38, 42 km)	26 (2)
2	CanAM4	1.0, 0.5 hPa (48, 54 km)	35 (3)
3	CCSM4	3.6, 2.2 hPa (38, 42 km)	26 (2)
4	CNRM-CM5**	10.0, 0 hPa (31, ∞ km)	31 (1)
5	GFDL-CM3	0.02, 0.01 hPa (76, 80 km)	48 (13)
6	GFDL-ESM2M	3.7, 1.0 hPa (38, 48 km)	24 (1)
7	GISS-E2-R	0.14, 0.10 hPa (64, 66 km)	40 (8)
8	HadGEM2-A	3.2, 2.1 hPa (39, 42 km)	38 (2)
9	INMCM4	10.0, 0 hPa (31, ∞ km)	21 (1)
10	IPSL-CM5A-LR	0.04, 0 hPa (72, ∞ km)	39 (9)
11	IPSL-CM5A-MR	0.04, 0 hPa (72, ∞ km)	39 (9)
12	MIROC5	2.9, 0 hPa (40, ∞ km)	40 (2)
13	MIROC-ESM	0.004, 0 hPa (86, ∞ km)	80 (33)
14	MIROC-ESM-CHEM	0.004, 0 hPa (86, ∞ km)	80 (33)
15	MRI-CGCM3	0.01, 0 hPa (80, ∞ km)	48 (11)
16	NorESM1-M	3.6, 2.2 hPa (38, 42 km)	26 (2)
17	WACCM4	$6, 5 \times 10^{-6}$ hPa (144, 148 km)	66 (18)

* Total number of vertical layers and, in parentheses, number of layers at altitudes with large solar UV absorption by ozone ($30 < z < 70$ km).

** Previous version (CNRM-CM3) had the highest full level of all CMIP3 models: 0.05 hPa (76 km; Déqué et al. 1994; Randall et al. 2007). For CMIP5, "it has been decided to reduce the number of levels because of constraints on computing resources..." (Voldoire et al. 2013).

Panel on Climate Change Fourth Assessment Report (IPCC AR4)–Coupled Model Intercomparison Project, phase 3 (CMIP3); Meehl et al. 2007]. Both CDML and the present study examine the surface pressure signature of the tides. Analogous to oceanic tides, atmospheric tides appear as oscillations of vertically integrated fluid mass—that is, of surface pressure (thus reflecting large-scale dynamics more than local effects). The CMIP3 database, however, included sea level pressure but not actual surface pressure in its high-time-frequency fields. Comparison of observed surface pressure with model-generated sea level pressure was problematic over elevated terrain, where the concept of equivalent sea level pressure is ambiguous. Fortunately a new version of the database includes surface pressure at 3-hourly frequency (IPCC AR5–CMIP5; Taylor et al. 2012). The new database also incorporates the latest generation of climate models, which cover a greater altitude range (Table 1).

Table 1 here is the analog of CDML's Table 1 but with a more careful definition of model top. Models use staggered vertical levels with one set ("layer midpoints" or "full levels") carrying temperature and other thermodynamic fields and a second set ("layer interfaces" or "half levels") carrying vertical velocity and other flux fields. Vertical coordinates are pressure based from the middle stratosphere upward. Several of the models put their topmost half level at zero pressure; using half levels to define model tops would imply that these models extend infinitely upward. Therefore we use full rather than half levels to define the vertical extent of models. (This leaves half of a model layer above the model top defined here. Ozone heating could occur in this half layer, but models with limited vertical extent generally suppress it in order to avoid unrealistic temperatures in the lower stratosphere.) We consider 23 CMIP5 models featured in recent studies of stratospheric dynamics (Driscoll et al. 2012; Wilcox et al. 2012; Charlton-Perez et al. 2013; Marsh et al. 2013). Three-hourly output has not been provided (or not provided in standard form) from 6 of these models, leaving 17 for this study. Ten of our 17 models include all of the stratosphere (topmost full level ≥ 48 km). Five include all of the stratosphere and mesosphere (topmost full level ≥ 76 km). In CMIP3, the corresponding fractions were 5/23 all stratosphere and 0/23 all stratosphere and mesosphere (Cordero and Forster 2006). One model [the Whole Atmosphere Community Climate Model, version 4 (WACCM4)] has by far the highest full level in CMIP5, extending well into the thermosphere.

2. Comparison with observations

Here we compare CMIP5 model output with the observed surface pressure data employed by CDML (Dai and Wang 1999). These remain the best high-frequency direct observations. Future studies may examine reanalysis of the direct observations via initialization algorithms for numerical weather prediction (NWP, which has produced reasonable tidal oscillations; see, e.g., Ray and Ponte 2003). For the present work, we choose the direct observations to permit direct comparison of the present results with CDML.

For the same reason (i.e., for direct comparison of the present results with CDML) we process the model output in exactly the same way. Observations of December–February for 1976–97 are compared with model output for 1 January–1 February 2000 inclusive (giving an exact power of 2 time points as input to fast Fourier transforms). CDML's appendix shows that, unlike the tides' upper-atmospheric signature (e.g., Burrage et al. 1995; Wu et al. 2008), surface pressure tide variations exhibit only small interannual variability.

a. Tide amplitude

Figures 1 and 2 show maps of CMIP5 diurnal and semidiurnal tide amplitudes, using the same color scales as the corresponding CMIP3 maps (CDML, their Figs. 2 and 3, respectively). For these figures, we selected one model with a typical placement of levels [Community Climate System Model, version 4 (CCSM4)] together

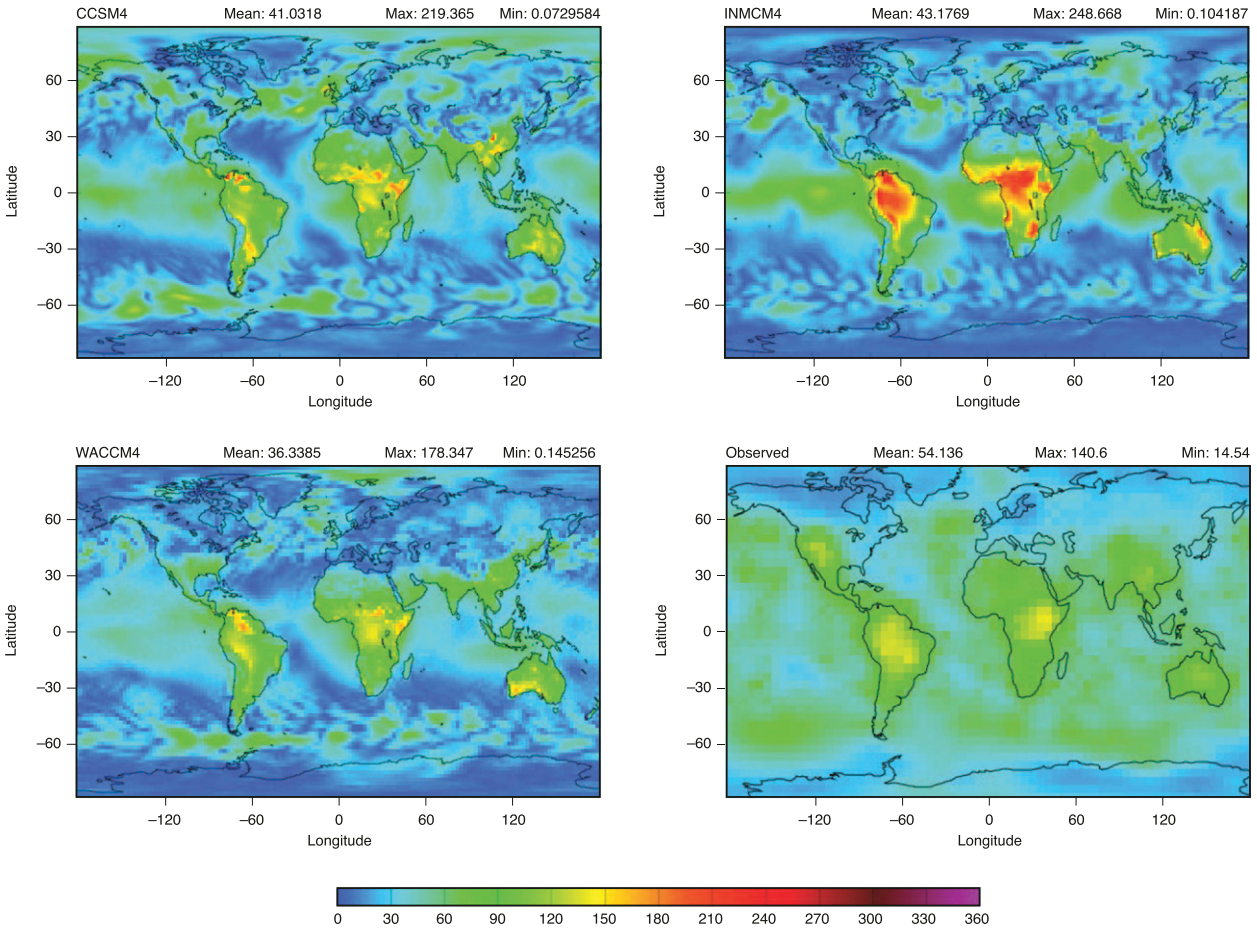

FIG. 1. Amplitudes (Pa) of diurnal harmonics of January surface pressure from (top),(bottom left) three CMIP5–IPCC-AR5 climate models and (bottom right) observations (Dai and Wang 1999).

with one of the two lowest-top models [Institute of Numerical Methods of the Russian Academy of Sciences, Climate Model, version 4 (INMCM4)] and the highest-top (WACCM4) model. Results from observations and all 17 models are presented in the online supplemental material. Only January results are shown to save space; July results are similar (see Table 2 and supplemental material).

WACCM4 is a ''superset'' of CCSM4 with added levels in the middle and upper atmosphere but identical subgrid-scale parameterizations in the troposphere (Marsh et al. 2013). Diurnal tide amplitude maps for WACCM4 and CCSM4 look quite similar (Fig. 1) while WACCM4 has greater semidiurnal amplitudes in the tropics (Fig. 2). This result is consistent with the theory of vertical propagation of the tides (Chapman and Lindzen 1970, their section 3.5; Holton 1975, their section 4.5). The diurnal harmonic is vertically trapped and therefore forced mostly by water vapor heating and other surface/tropospheric processes. The semidiurnal harmonic is forced mostly by ozone heating around 30–70-km altitude—a region that CCSM4 does not fully include. Therefore, CCSM4 obtains less semidiurnal amplitude than WACCM4. As a result, CCSM4 agrees better with observations of the semidiurnal tide. But (as shown below and in CDMS), all CMIP models overpredict tidal amplitudes at low latitudes, so reducing tidal amplitude can ''improve'' model results by means of cancelling errors.

Semidiurnal tide amplitudes are particularly surprising in the Centre National de Recherches Météorologiques Coupled Global Climate Model, version 5 (CNRM-CM5), and INMCM4, which have the lowest model tops. In the tropics, INMCM4's diurnal harmonic is less accurate than CCSM4 and WACCM4 (Fig. 1), but its semidiurnal harmonic is about as accurate as CCSM4's and thus more accurate than WACCM4's (Fig. 2). Table 2 (analogous to CDML's Table 3) includes CNRM, as well as CCSM, INMCM, and WACCM. It shows three comparisons of tide amplitude: the global mean of model–observed amplitude ratio R, the model-observed spatial

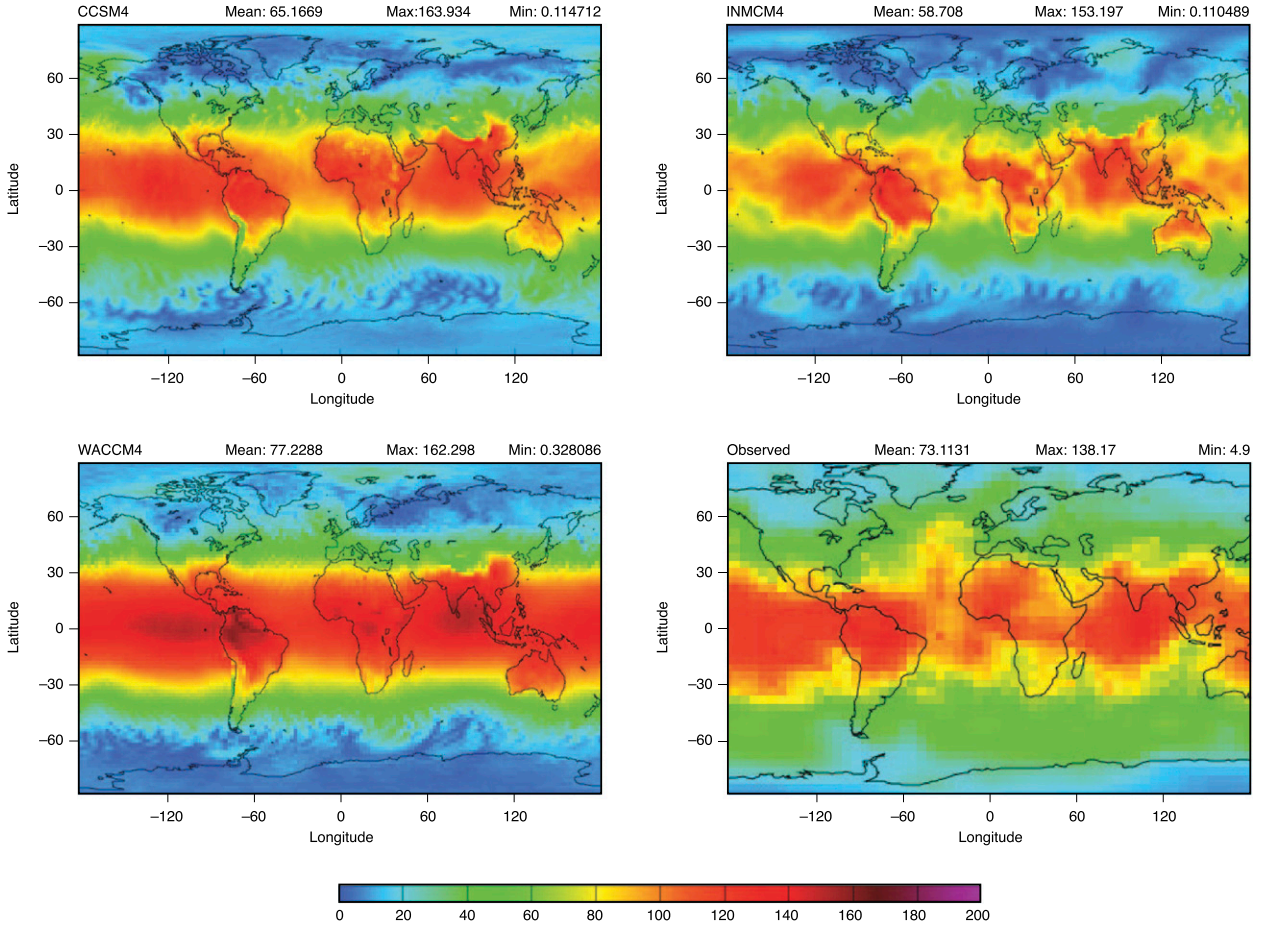

FIG. 2. As in Fig. 1, but for the semidiurnal harmonics; note different color scale.

correlation ρ, and the model-observed root-mean-square difference Δ. [A fourth measure, the model–observed ratio of variances, is dependent on ρ and Δ; it is often shown in a two-dimensional Taylor (2001) diagram that omits R.] Generally comparable performance of the CMIP5 models is evident. For CNRM-CM5, errors in terms of Δ are somewhat greater than in the other models, but a look at R indicates that part of the problem comes from overprediction of the semidiurnal amplitude. The overprediction is obvious in corresponding amplitude maps (see Fig. S4 in the supplemental material).

In addition to the models discussed above, Table 2 includes the CMIP3 analogs of CNRM-CM5 and INMCM4: CNRM-CM3 and INMCM3 respectively. CNRM-CM3 had the highest top of the CMIP3 models examined by CDML, but the topmost full level in CNRM-CM5 is lowered to the 10-hPa pressure level, the same as INMCM's (Table 1). Table 2 does not suggest any substantial difference in the quality of tide simulations between the two versions of CNRM-CM.

Since both INMCM3 and INMCM4 have identically placed vertical levels, comparing the two shows the advantages of using actual surface pressure in CMIP5 tide studies. The INMCM4 diurnal harmonic amplitude map (Fig. 1) differs noticeably from INMCM3 (CDML, their Fig. 2) by exhibiting less excessively large amplitudes; the maximum value (>360 Pa) has been reduced to a more reasonable 249 Pa (versus an observed maximum value of 141 hPa). For the semidiurnal harmonic (Fig. 2) INMCM4 reduces some excessive amplitude values that appeared over tropical land areas, bringing the maximum value into better agreement with observation (cf. CDML, their Fig. 3). All of these improvements are likely due to the use of actual surface pressure in the CMIP5 database. The use of sea level pressure inflated INMCM3's amplitude at low latitudes, making up for an underestimate of amplitude at higher latitudes (see Figs. 2–3 in CDML). Thus INMCM4's "worse" values of global-mean R are not meaningful. The other numbers are about the same in the two versions of INMCM except for Δ, which is substantially lowered in INMCM4's diurnal harmonics.

TABLE 2. Comparison of observed surface pressure tide amplitude with simulations from selected CMIP5–IPCC AR5 models (CCSM4, WACCM4, CNRM-CM5, and INMCM4: surface pressure output, unmasked) and CMIP3–IPCC AR4 models (CNRM-CM3 and INMCM3: sea level pressure output, masked). ''Unmasked'' means that the comparison is made over the entire surface area of Earth. ''Masked'' means that land areas with elevation greater than 1 km are excluded from the comparison. INMCM3 and CNRM-CM3 values are repeated from Table 3 in CDML.

Model	Harmonic	Month	$R \equiv$ Global-mean model–obs ratio	$\rho \equiv$ Model–obs correlation	$\Delta \equiv$ Model – obs rms difference (Pa)
CCSM4	Diurnal	January	0.777	0.592	27.5
WACCM4			0.658	0.692	26.6
CCSM4		July	0.822	0.511	28.7
WACCM4			0.745	0.549	27.8
CCSM4	Semidiurnal	January	0.832	0.930	16.6
WACCM4			0.950	0.942	21.1
CCSM4		July	0.790	0.910	17.1
WACCM4			0.965	0.907	20.2
CNRM-CM3	Diurnal	January	0.843	0.733	33.4
CNRM-CM5			0.795	0.696	30.6
CNRM-CM3		July	0.809	0.753	29.1
CNRM-CM5			0.890	0.627	27.0
CNRM-CM3	Semidiurnal	January	0.997	0.929	24.1
CNRM-CM5			1.119	0.890	39.9
CNRM-CM3		July	1.021	0.890	24.6
CNRM-CM5			1.076	0.817	26.3
INMCM3	Diurnal	January	0.808	0.703	39.6
INMCM4			0.767	0.652	30.1
INMCM3		July	0.944	0.739	39.9
INMCM4			0.786	0.622	28.1
INMCM3	Semidiurnal	January	0.920	0.912	20.6
INMCM4			0.726	0.937	19.2
INMCM3		July	0.914	0.885	19.4
INMCM4			0.708	0.904	20.3

In short, although the models CNRM-CM5, INMCM4, CCSM4, and WACCM4 span the range of altitude coverage in CMIP5, with topmost full levels between 31 and 144 km, they exhibit relatively small differences in the accuracy of their tide amplitude simulations. These results are consistent with CDML and lend support to the hypothesis of ''compensating errors.''

b. *Wavenumbers, migrating components, and tide phase*

Figure 3 (analogous to CDML's Fig. 8a) shows, for January, the equatorial Fourier longitude-transformed amplitudes of all 17 CMIP5 models and observations as a function of zonal wavenumber s. This allows isolation of the ''migrating'' components of the tides that follow the apparent motion of the sun across the sky (i.e., $s = 1$ for the diurnal harmonic and $s = 2$ for the semidiurnal harmonic). The migrating components dominate both harmonics in models and observations, but all of the models overestimate migrating amplitudes (by up to a factor of 2). These results were also noted by CDML for the CMIP3 models. Also apparent both in Fig. 3 and in the analogous CMIP3 output are secondary peak diurnal amplitudes at $s = -3$ and $+5$, representing eastward- and westward-propagating waves, respectively, with respect to the diurnal migrating component. The combination of secondary waves is mathematically equivalent to the product of a migrating diurnal tide and a stationary wave with $s = 4$ (i.e., $1 \pm 4 = -3$ or $+5$; cf. Forbes and Hagan 2000). These secondary waves are observed in the upper atmosphere, arising from $s = 4$ forcing by topography and land–sea heating contrasts (Zhang et al. 2006). As with the migrating tides, their surface pressure signatures are overestimated by the models.

Figure 4 shows, for January, the zonal vector-mean values of the local time of maximum surface pressure for all 17 CMIP5 models and observations as a function of latitude. July results (not shown) are similar. This is one measure of the phase of the tides. CDML showed a somewhat different measure: the phase of the migrating component obtained by Fourier analysis (see preceding subsection and CDML's Fig. 4). While isolating the migrating component makes a connection to classical

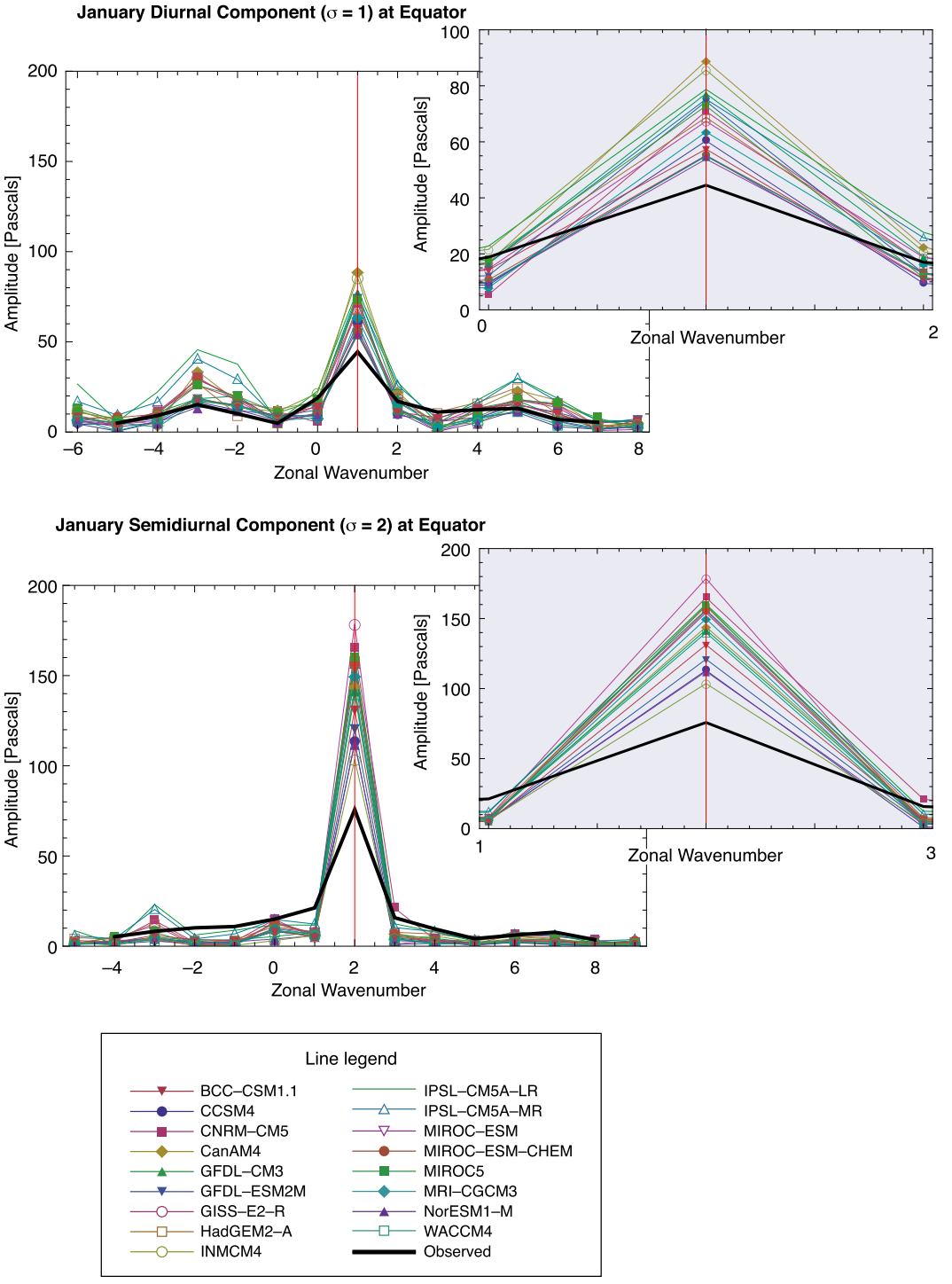

FIG. 3. Fourier amplitude at the equator vs zonal wavenumber for (top) diurnal and (bottom) semidiurnal harmonics of all CMIP5–IPCC AR5 climate models in this study (thin colored lines) and observations for January (thick black line). Closeups show details of peaks in the vicinity of migrating Fourier-component wavenumbers (red vertical lines).

linear tide theory (Chapman and Lindzen 1970), it does not allow direct comparison with observations (Dai and Wang 1999) since the latter includes phase information only for the combination of all zonal wavenumbers. Phase diagrams for the migrating components of CMIP5 tides (not shown here) strongly resemble their CMIP3 analogs and deliver the same basic message as Fig. 4.

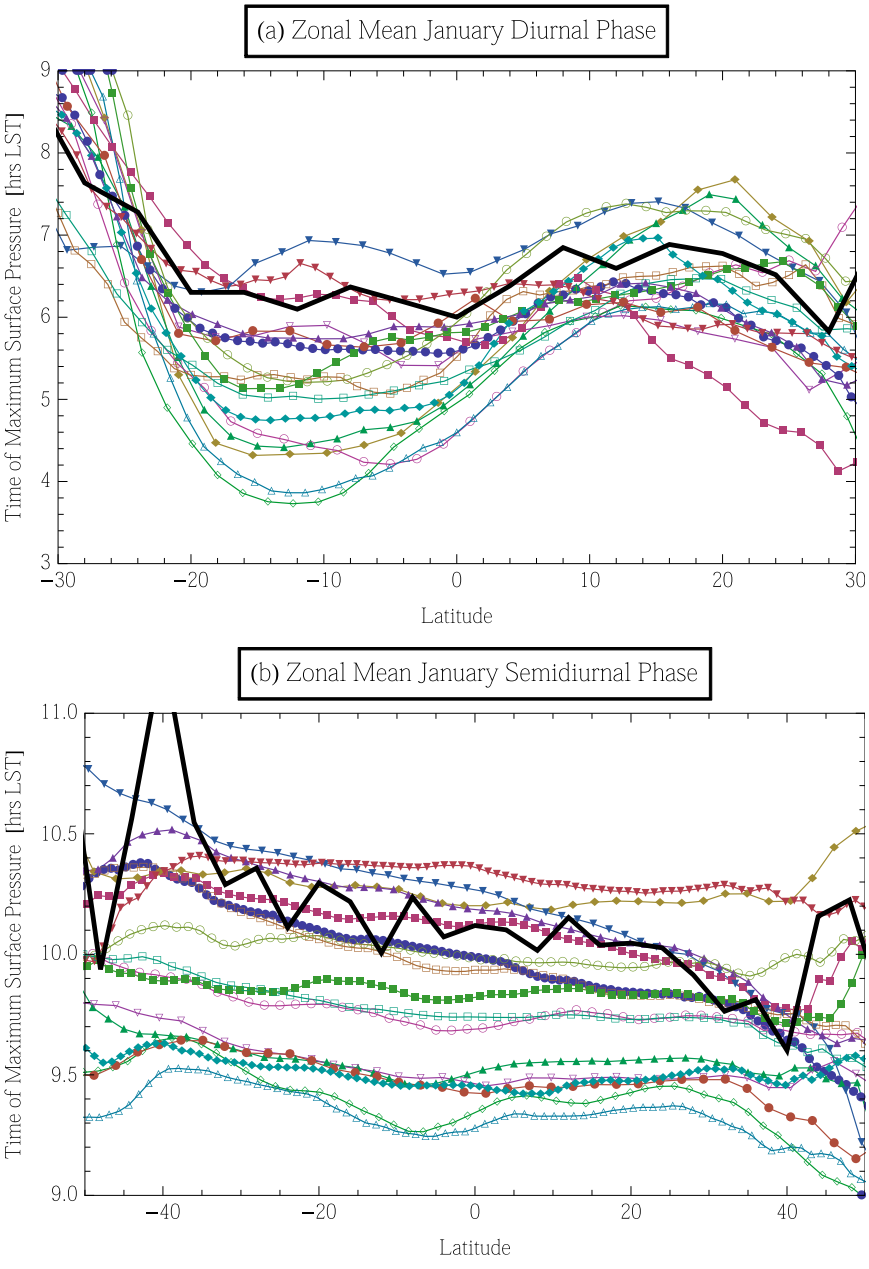

FIG. 4. January tidal phase vs latitude for observations (thick black line) and for all CMIP5–IPCC AR5 climate models in this study (colored lines). See Fig. 3 for line legend distinguishing the different models. (a) Diurnal and (b) semidiurnal harmonics are shown only for low latitudes, at which tidal amplitude is significant and therefore tidal phase is well defined. Note different latitude scales in (a) and (b).

The message (as in CDML) is that in the tropics, where tidal amplitude is strongest, model-simulated times of maximum are roughly 0600 LST for the diurnal harmonic and 1000 and 2200 LST for the semidiurnal harmonic. This agrees approximately with observations, but Fig. 4 shows the simulated times of maximum are generally earlier than observed. The discrepancy is up to about 1 h in the semidiurnal harmonic and about 2 h in the diurnal harmonic, depending on the model. As with tidal amplitude, there is no obvious correlation between the accuracy of model-simulated phase and the model's vertical domain. For example, the six models producing the most accurate semidiurnal phase near the equator are INMCM4, CNRM-CM5, CCSM4,

Norwegian Earth System Model, version 1(NorESM1), Hadley Centre Global Environmental Model, version 2, Atmosphere configuration (HadGEM2-A), and Canadian Centre for Climate Modelling and Analysis (CCCma) fourth-generation atmospheric general circulation model (CanAM4). These models have topmost full levels at 31–48 km, in the lower range of the models studied here. The tidal phase may be related to the timing of the heating (which is unrelated to the model top), which is consistent with the suggestion of Lindzen (1978) that earlier-than-observed semidiurnal maxima could be corrected by better accounting of tropospheric latent heat release.

3. Conclusions

The approximate consistency of CMIP3 and CMIP5 tide simulations with each other and with observations occurs despite the fact that the lowest-top model (INMCM) extends only into the middle stratosphere, whereas the highest-top model (WACCM) extends well into the thermosphere. Some of the low-top models have part of one layer above the ''model top'' defined here, which could potentially include additional ozone heating. As noted in the introduction, however, it has been shown that lower-top models can produce compensating errors, with wave reflection from the model top making up for missing ozone forcing at higher altitudes (Lindzen et al. 1968; see also Zwiers and Hamilton 1986; Hamilton et al. 2008). It is not well documented how gravity waves interact with the tops of various models (which generally include parameterizations to minimize artificial reflection), but the CMIP5 database now provides an ''apples to apples'' comparison with observations in terms of actual surface pressure that further supports the compensating errors hypothesis for the semidiurnal harmonic. Confirmation of the hypothesis, however, will require direct examination of wave propagation in and above the ozone layer (e.g., classical linear calculations with vertical discretization matching the various CMIP models). Analyses of the ozone heating profiles and wave reflection in the CMIP models may also help settle this issue.

Other future work could focus on near-surface processes or go beyond the surface signature of the tides and examine free-atmosphere fields. For the diurnal harmonic of surface pressure, both classical tide theory and comparison of the two CMIP5 models with identical troposphere formulations (Fig. 1) indicate forcing by lower-atmospheric processes, including sensible heating from the ground as noticed by Dai and Wang (1999). Near-surface temperature, humidity, winds, and other model output fields provided at 3-hourly frequency in the CMIP5 database would provide additional insight about such processes [as in Dai and Trenberth (2004) for one model], as well as information relevant to practical human and ecological concerns. In addition, CMIP5 provides temperature, winds, and humidity on all model levels at 6-hourly frequency. This should suffice for study of the (dominant) diurnal tide harmonic in and above the stratosphere. In a broader sense, the extension of CMIP5 models to include the middle atmosphere (Table 1) offers a new domain of climate model intercomparison.

Acknowledgments. We appreciate reviewers stressing the distinction between diurnal and semidiurnal tide forcing. We acknowledge the Working Group on Coupled Modeling, which oversees CMIP, and thank the climate modeling groups (Table 1) for their output. For CMIP, the U.S. Department of Energy's Program for Climate Model Diagnosis and Intercomparison provides coordinating support and software infrastructure in partnership with the Global Organization for Earth System Science Portals. This work was performed under auspices of the DOE Office of Science by Lawrence Livermore National Laboratory under Contract DE-AC52-07NA27344 and at the National Center for Atmospheric Research.

REFERENCES

Burrage, M. D., M. E. Hagan, W. R. Skinner, D. L. Wu, and P. B. Hays, 1995: Long-term variability in the solar diurnal tide observed by HRDI and simulated by the GSWM. *Geophys. Res. Lett.,* **22,** 2641–2644, doi:10.1029/95GL02635.

Chapman, S., and R. S. Lindzen, 1970: *Atmospheric Tides.* D. Reidel, 200 pp.

Charlton-Perez, A. J., and Coauthors, 2013: On the lack of stratospheric dynamical variability in low-top versions of the CMIP5 models. *J. Geophys. Res.,* **118,** 2494–2505, doi:10.1002/jgrd.50125.

Cordero, E. C., and P. M. de F. Forster, 2006: Stratospheric variability and trends in models used for the IPCC AR4. *Atmos. Chem. Phys.,* **6,** 5369–5380, doi:10.5194/acp-6-5369-2006.

Covey, C., A. Dai, D. Marsh, and R. S. Lindzen, 2011: The surface-pressure signature of atmospheric tides in modern climate models. *J. Atmos. Sci.,* **68,** 495–514, doi:10.1175/2010JAS3560.1.

Dai, A., and J. Wang, 1999: Diurnal and semidiurnal tides in global surface pressure fields. *J. Atmos. Sci.,* **56,** 3874–3890, doi:10.1175/1520-0469(1999)056<3874:DASTIG>2.0.CO;2.

——, and K. E. Trenberth, 2004: The diurnal cycle and its depiction in the Community Climate System Model. *J. Climate,* **17,** 930–951, doi:10.1175/1520-0442(2004)017<0930:TDCAID>2.0.CO;2.

Déqué, M., C. Dreveton, A. Braun, and D. Cariolle, 1994: The ARPEGE/IFS atmosphere model—A contribution to the French community climate modeling. *Climate Dyn.,* **10,** 249–266, doi:10.1007/BF00208992.

Driscoll, S., A. Bozzo, L. J. Gray, A. Robock, and G. Stenchikov, 2012: Coupled Model Intercomparison Project 5 (CMIP5) simulations of climate following volcanic eruptions. *J. Geophys. Res.,* **117,** D17105, doi:10.1029/2012JD017607.

Forbes, J. M., and M. E. Hagan, 2000: Diurnal Kelvin wave in the atmosphere of Mars: Towards an understanding of ''stationary'' density structures observed by the MGS

accelerometer. *Geophys. Res. Lett.,* **27,** 3563–3566, doi:10.1029/2000GL011850.

Hamilton, K., S. C. Ryan, and W. Ohfuchi, 2008: Orographic effects on the solar semidiurnal surface tide simulated in a very fine resolution general circulation model. *J. Geophys. Res.,* **113,** D17114, doi:10.1029/2008JD010115.

Holton, J. R., 1975: *The Dynamical Meteorology of the Stratosphere and Mesosphere*. Amer. Meteor. Soc., 216 pp.

Lindzen, R. S., 1978: Effect of daily variations of cumulonimbus activity on the atmospheric semidiurnal tide. *Mon. Wea. Rev.,* **106,** 526–533, doi:10.1175/1520-0493(1978)106<0526:EODVOC>2.0.CO;2.

——, E. S. Batten, and J.-W. Kim, 1968: Oscillations in atmospheres with tops. *Mon. Wea. Rev.,* **96,** 133–140, doi:10.1175/1520-0493(1968)096<0133:OIAWT>2.0.CO;2.

Marsh, D. R., M. Mills, D. Kinnison, J.-F. Lamarque, N. Calvo, and L. Polvani, 2013: Climate change from 1850 to 2005 simulated in CESM1(WACCM). *J. Climate,* **26,** 7372–7391, doi:10.1175/JCLI-D-12-00558.1.

Meehl, G. A., C. Covey, T. Delworth, M. Latif, B. McAvaney, J. F. B. Mitchell, R. J. Stouffer, and K. E. Taylor, 2007: The WCRP CMIP3 multimodel dataset: A new era in climate change research. *Bull. Amer. Meteor. Soc.,* **88,** 1383–1394, doi:10.1175/BAMS-88-9-1383.

Randall, D. A., and Coauthors, 2007: Climate models and their evaluation. *Climate Change 2007: The Physical Science Basis,* S. Solomon et al., Eds., Cambridge University Press, 589–662.

Ray, R. D., and R. M. Ponte, 2003: Barometric tides from ECMWF operational analyses. *Ann. Geophys.,* **21,** 1897–1910, doi:10.5194/angeo-21-1897-2003.

Taylor, K. E., 2001: Summarizing multiple aspects of model performance in a single diagram. *J. Geophys. Res.,* **106,** 7183–7192, doi:10.1029/2000JD900719.

——, R. J. Stouffer, and G. A. Meehl, 2012: An overview of CMIP5 and the experiment design. *Bull. Amer. Meteor. Soc.,* **93,** 485–498, doi:10.1175/BAMS-D-11-00094.1.

Voldoire, A., and Coauthors, 2013: The CNRM-CM5.1 global climate model: Description and basic evaluation. *Climate Dyn.,* **40,** 2091–2121, doi:10.1007/s00382-011-1259-y.

Wilcox, L. J., A. J. Charlton-Perez, and L. J. Gray, 2012: Trends in Austral jet position in ensembles of high- and low-top CMIP5 models. *J. Geophys. Res.,* **117,** D13115, doi:10.1029/2012JD017597.

Wu, Q., and Coauthors, 2008: Global distribution and interannual variations of mesospheric and lower thermospheric neutral wind diurnal tide: 1. Migrating tide. *J. Geophys. Res.,* **113,** A05308, doi:10.1029/2007JA012542.

Zhang, X., J. M. Forbes, M. E. Hagan, J. M. Russell III, S. E. Palo, J. Mertens, and M. G. Mlynczak, 2006: Monthly tidal temperatures 20–120 km from TIMED/SABER. *J. Geophys. Res.,* **111,** A10S08, doi:10.1029/2005JA011504.

Zwiers, F., and K. Hamilton, 1986: Simulation of solar tides in the Canadian Climate Center General Circulation Model. *J. Geophys. Res.,* **91,** 11 877–11 896, doi:10.1029/JD091iD11p11877.